

## Poly(glycerol monomethacrylate)-Poly(benzyl methacrylate) Diblock Copolymer Nanoparticles via RAFT Emulsion Polymerization: Synthesis, Characterization, and Interfacial Activity

Victoria J. Cunningham, Abdullah M. Alswieleh, Kate L. Thompson, Mark Williams, Graham J. Leggett, and Steven P. Armes\*

Department of Chemistry, University of Sheffield, Brook Hill, Sheffield, South Yorkshire S3 7HF, U.K.

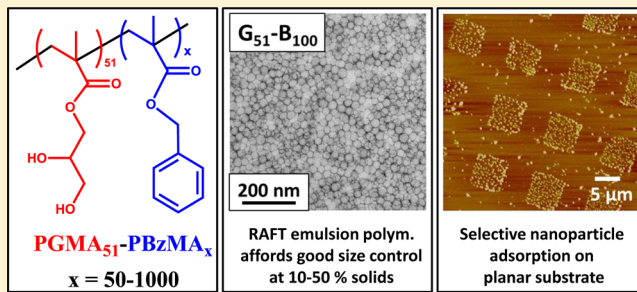
Osama M. Musa

Ashland Specialty Ingredients, 1005 US 202/206, Bridgewater, New Jersey 08807, United States

### S Supporting Information

**ABSTRACT:** A poly(glycerol monomethacrylate) (PGMA) macromolecular chain transfer agent has been utilized to polymerize benzyl methacrylate (BzMA) via reversible addition–fragmentation chain transfer (RAFT)-mediated aqueous emulsion polymerization. This formulation leads to the efficient formation of spherical diblock copolymer nanoparticles at up to 50% solids. The degree of polymerization (DP) of the core-forming PBzMA block has been systematically varied to control the mean particle diameter from 20 to 193 nm. Conversions of more than 99% were achieved for PGMA<sub>51</sub>-PBzMA<sub>250</sub> within 6 h at 70 °C using

macro-CTA/initiator molar ratios ranging from 3.0 to 10.0. DMF GPC analyses confirmed that relatively low polydispersities ( $M_w/M_n < 1.30$ ) and high blocking efficiencies could be achieved. These spherical nanoparticles are stable to both freeze–thaw cycles and the presence of added salt (up to 0.25 M MgSO<sub>4</sub>). Three sets of PGMA<sub>51</sub>-PBzMA<sub>x</sub> spherical nanoparticles have been used to prepare stable Pickering emulsions at various copolymer concentrations in four model oils: sunflower oil, *n*-dodecane, *n*-hexane, and isopropyl myristate. A reduction in mean droplet diameter was observed via laser diffraction on increasing the nanoparticle concentration. Finally, the cis diol functionality on the PGMA stabilizer chains has been exploited to demonstrate the selective adsorption of PGMA<sub>51</sub>-PBzMA<sub>100</sub> nanoparticles onto a micropatterned phenylboronic acid-functionalized planar surface. Formation of a cyclic boronate ester at pH 10 causes strong *selective* binding of the nanoparticles via the *cis*-diol groups in the PGMA stabilizer chains, as judged by AFM studies. Control experiments confirmed that minimal selective nanoparticle binding occurred at pH 4, or if the PGMA<sub>51</sub> stabilizer block was replaced with a poly(ethylene glycol) PEG<sub>113</sub> stabilizer block.



### INTRODUCTION

Conventional aqueous emulsion polymerization requires a water-immiscible monomer, a water-soluble initiator, surfactant and water. Such environmentally-friendly formulations are widely utilized for the industrial manufacture of many polymers in latex form, since they offer a number of practical advantages.<sup>1,2</sup> They are applicable to a wide range of vinyl monomers, enable highly efficient polymerizations to be conducted at high solids with relatively low solution viscosities, and allow high molecular weights to be targeted. However, one disadvantage of conventional emulsion polymerization is that particle size is directly related to the surfactant concentration. Thus nanosized latexes require relatively high surfactant concentrations, which can be detrimental to the performance of the final polymer product. For example, excess surfactant can migrate within latex films, leading to reduced interfacial adhesion and poor transparency.<sup>3</sup>

In principle, controlled/“living” radical polymerization techniques such as nitroxide-mediated polymerization (NMP),<sup>4,5</sup> atom transfer radical polymerization (ATRP)<sup>6</sup> or reversible addition–fragmentation chain transfer polymerization (RAFT)<sup>7</sup> offer several advantages over conventional free radical polymerization. In particular, the recent development of RAFT aqueous emulsion polymerization<sup>8,9</sup> offers a potential surfactant-free route for the efficient synthesis of nanosized latexes. Early RAFT aqueous emulsion polymerizations involved the addition of a RAFT agent to a conventional emulsion polymerization. Such formulations suffered from many problems, including poor molecular weight control, colloidal instability and substantially incomplete

Received: June 2, 2014

Revised: July 16, 2014

Published: August 14, 2014



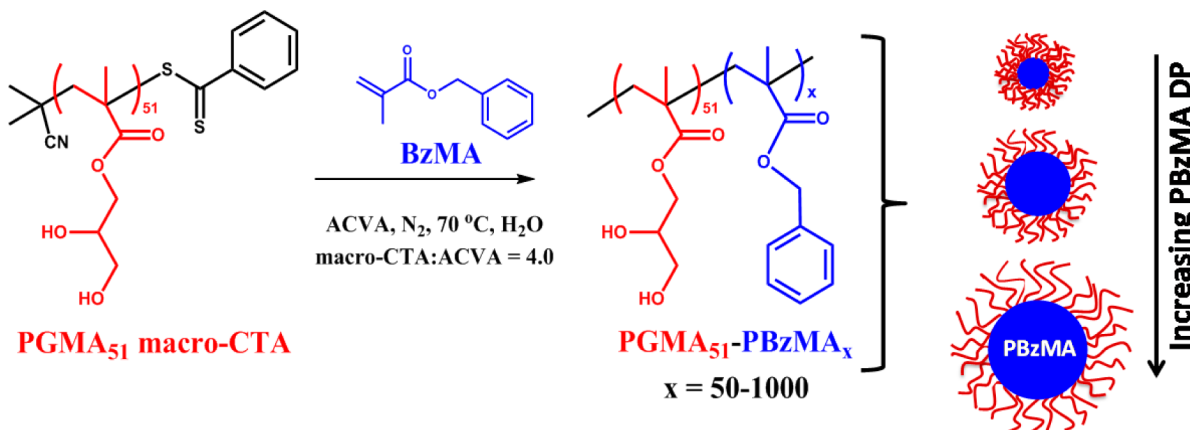


**Figure 1.** Synthesis of  $\text{PGMA}_{51}-\text{PBzMA}_x$  diblock copolymer nanoparticles via RAFT aqueous emulsion polymerization. The spherical particle diameter increases monotonically on increasing the target degree of polymerization of the core-forming PBzMA block.

monomer conversions.<sup>10</sup> These problems were addressed, at least in part, by developing a seeded RAFT emulsion polymerization protocol.<sup>11</sup> However, the initial latex seed was not formed via RAFT polymerization, hence the final polymers did not exhibit low polydispersities or exhibit controlled molecular weights. Hawkett et al. developed the first successful *ab initio* RAFT emulsion polymerization using a poly(acrylic acid) macromolecular chain transfer agent (macro-CTA), which was chain-extended using *n*-butyl acrylate to form stable latex particles.<sup>12–14</sup> This formulation was further developed to produce ABC triblock copolymers by the addition of styrene as the third block.<sup>15</sup>

More recently, Charleux and co-workers developed robust RAFT emulsion polymerization protocols in a series of pioneering studies. A range of hydrophilic stabilizer blocks (acrylic,<sup>16–18</sup> methacrylic,<sup>19</sup> and acrylamide<sup>20</sup>), hydrophobic core-forming blocks (*n*-butyl acrylate,<sup>20</sup> styrene,<sup>19,21,22</sup> methyl methacrylate,<sup>23</sup> and benzyl methacrylate<sup>24</sup>) and RAFT agents (both trithiocarbonates<sup>16,20</sup> and dithiobenzoates<sup>19</sup>) were evaluated, and other parameters such as solution pH<sup>18,22</sup> were studied in detail. Various formulations were optimized to provide high final monomer conversions, narrow molecular weight distributions and good control over the copolymer morphology. The first example of RAFT emulsion polymerization to yield nonspherical nano-objects involved a poly-(acrylic acid-*co*-poly(ethylene oxide) methyl ether acrylate) macro-CTA prepared using a trithiocarbonate RAFT agent. This water-soluble precursor was chain-extended using styrene to form a series of diblock copolymer nanoparticles.<sup>16</sup> Polymerization-induced self-assembly (PISA) led to the formation of spheres, fibers or vesicles depending mainly on the target degree of polymerization of the polystyrene block, although other parameters such as the stirring speed, solution pH and salt concentration were also shown to be important.<sup>17</sup> Replacing this acrylic macro-CTA with the equivalent methacrylic macro-CTA for the polymerization of styrene, along with the construction of suitable phase diagrams, enabled pure sphere, fiber or vesicle phases to be reproducibly targeted for a given steric stabilizer composition.<sup>25</sup> A further refinement was the development of a wholly aqueous one-pot formulation, in which the synthesis of the macro-CTA precursor was combined with that of the sterically-stabilized nanoparticles.<sup>21,26–28</sup> A comprehensive review article summarizing the development of this field was published in 2012.<sup>8</sup> In most literature examples of RAFT emulsion polymerization, the

steric stabilizer contains (meth)acrylic acid comonomer and therefore has appreciable *anionic* character. Indeed, we are aware of just five reports describing the use of a *non-ionic* steric stabilizer (typically a poly(ethylene oxide) macro-CTA).<sup>23,29–32</sup>

Notwithstanding the intensive research on RAFT emulsion polymerization summarized above, the present work describes a relatively rare example of a RAFT aqueous emulsion polymerization formulation based on a *non-ionic* steric stabilizer block, poly(glycerol monomethacrylate) (PGMA). Glycerol monomethacrylate (GMA) is a relatively expensive specialty monomer, but we have recently reported its cost-effective synthesis from glycidyl methacrylate, which is a cheap commodity monomer. In the present work, two PGMA macro-CTAs have been chain-extended using a water-immiscible monomer, benzyl methacrylate (BzMA), via RAFT aqueous emulsion polymerization, see Figure 1. The effect of varying the target degree of polymerization of the core-forming PBzMA block and the overall copolymer concentration on the particle size, blocking efficiency and conversion has been systematically investigated. Moreover, these new  $\text{PGMA}_{51}-\text{PBzMA}_x$  nanoparticles are also assessed as putative Pickering emulsifiers for four model oils. Finally, the dihydroxy functionality of the PGMA stabilizer chains has been exploited to control the surface adsorption of the  $\text{PGMA}_{51}-\text{PBzMA}_{100}$  nanoparticles on a micropatterned planar substrate via phenylboronic acid chemistry.<sup>33–35</sup>

## EXPERIMENTAL SECTION

**Materials.** Glycerol monomethacrylate (GMA) was donated by GEO Specialty Chemicals (Hythe, U.K.) and used without further purification. Benzyl methacrylate (BzMA), 4,4'-azobis(4-cyanopentanoic acid) (ACVA; 99%), *n*-dodecane, isopropyl myristate, sunflower oil and 3-formylphenylboronic acid were purchased from Sigma-Aldrich U.K. and were used as received. 2-Cyano-2-propyl dithiobenzoate (CPDB) was purchased from STREM Chemicals Ltd. (Cambridge, U.K.) and was used as received. Dimethyl sulfoxide-*d*<sub>6</sub>, dimethylformamide-*d*<sub>7</sub> and methanol-*d*<sub>4</sub> were purchased from Goss Scientific Instruments Ltd. (Cheshire, U.K.) All other solvents were purchased from Fisher Scientific (Loughborough, U.K.) and used as received. Deionized water was used for all experiments.

**Preparation of  $\text{PGMA}_{51}$  Macro-CTA.** CPDB RAFT agent (1.650 g, 7.454 mmol), GMA (78.144 g, 488 mmol), and ACVA (0.3790 g, 1.352 mmol; CPDB/ACVA molar ratio = 5.0) were weighed into a 500 mL round-bottom flask and degassed with nitrogen for 15 min. Ethanol (148 mL) was deoxygenated separately with nitrogen for 30 min prior to addition to the other reagents. The reaction solution was

stirred and degassed in an ice bath for a further 30 min before placing in an oil bath at 70 °C. The polymerization was allowed to proceed for 150 min, resulting in a monomer conversion of 68% as judged by <sup>1</sup>H NMR. The crude homopolymer was purified by precipitating into a 10-fold excess of dichloromethane from methanol. This purification process was repeated twice to give a pure PGMA macro-CTA (53.14 g, < 1% monomer remaining). The mean degree of polymerization was calculated to be 51 as judged by <sup>1</sup>H NMR. DMF GPC analysis indicated an  $M_n$  of 15 000 g mol<sup>-1</sup> and an  $M_w/M_n$  of 1.19 (vs a series of near-monodisperse poly(methyl methacrylate) (PMMA) calibration standards).

**RAFT Aqueous Emulsion Polymerization of Benzyl Methacrylate.** A typical protocol for the synthesis of PGMA<sub>51</sub>–PBzMA<sub>300</sub> diblock copolymer was as follows: PGMA<sub>51</sub> macro-CTA (0.0696 g), BzMA (0.4414 g, 2.505 mmol), ACVA (0.600 mg, 2.141 μmol; CTA/ACVA molar ratio = 4.0) and water (4.58 g, 10% w/w) were weighed into a 25 mL round-bottom flask and purged with nitrogen for 30 min, prior to immersion in an oil bath set at 70 °C for 6 h. The resulting copolymer was analyzed by DMF GPC ( $M_n$  = 62 100 g mol<sup>-1</sup>,  $M_w/M_n$  = 1.18 vs PMMA standards). <sup>1</sup>H NMR spectroscopy analysis of a freeze-dried sample dissolved in DMSO-*d*<sub>6</sub> indicated less than 1% residual BzMA monomer. DLS studies of a 0.20% w/w copolymer dispersion indicated an intensity-average particle diameter of 91 nm (DLS polydispersity, PDI = 0.053).

**Synthesis of Fluorescently-Labeled PGMA<sub>51</sub>–PBzMA<sub>100</sub> Nanoparticles.** An excess of methylamine solution (33 wt % in absolute ethanol) was added to PGMA<sub>51</sub>–PBzMA<sub>100</sub> (1.50 g) synthesized via RAFT aqueous emulsion polymerization. After 10 min, this aqueous copolymer dispersion was reacted with rhodamine B isothiocyanate (3.10 mg, 5.78 μmol) for 40 h at 20 °C with continuous magnetic stirring. The resulting fluorescently-labeled nanoparticles were purified by dialysis for 8 days with 2–5 water changes per day. DLS studies of a 0.20% w/w copolymer dispersion indicated an intensity-average particle diameter of 46 nm (PDI = 0.15). The resulting copolymer was analyzed by DMF GPC ( $M_n$  = 29 200 g mol<sup>-1</sup>,  $M_w/M_n$  = 1.10 vs PMMA standards).

**Preparation of Pickering Emulsions Using PGMA–PBzMA Latex Particles.** Either sunflower oil, *n*-hexane, *n*-dodecane, or isopropyl myristate (2.0 mL) was homogenized with 2.0 mL of a 0.0675–2.50% w/w aqueous PGMA<sub>51</sub>–PBzMA<sub>x</sub> copolymer dispersion for 2 min using a IKA Ultra-Turrax T-18 homogenizer equipped with a 10 mm dispersing tool operating at 12 000 rpm.

**Preparation of Surface-Aminated Silicon Wafers Using (N-[2-(2-Nitrophenyl)propan-1-oxycarbonyl]-3-aminopropyl).** All glassware and substrates were cleaned by immersing them in “piranha” solution (a 3:7 mixture of hydrogen peroxide and concentrated sulfuric acid) for 2 h. (Caution! Piranha solution is an extremely strong oxidizing agent which has been known to detonate spontaneously upon contact with organic material). The glassware and the substrates were washed with deionized water several times, then sonicated for 10 min and rinsed with deionized water. Glassware and substrates were dried in a 120 °C oven for 1 h. The silicon wafers were submerged in a 1:1:5 solution of ammonium hydroxide, 30% hydrogen peroxide and deionized water (The Radio Cooperative America). The solution was heated to 85 °C for 30 min and allowed to cool. Samples were rinsed with deionized water, sonicated and dried in an oven before use.

Silicon wafers were immersed into a 1 mM solution of (N-[2-(2-nitrophenyl)propan-1-oxycarbonyl]-3-aminopropyl)triethoxysilane (NPPOC–silane) in toluene for 48 h at 20 °C. The coated wafers were rinsed with toluene, followed by ethanol, and dried under a stream of nitrogen gas.

**Photopatterning of NPPOC-Functionalized Surfaces.** A He–Cd laser (Kimmon IK3202R-D) with an UV emission wavelength of 325 nm was used to irradiate samples. The area illuminated by the laser beam was 0.20 cm<sup>2</sup> and the laser power was 11 mW. Micropatterns were obtained by irradiation of NPPOC-coated silicon wafers using an electron microscopy copper grid (Agar, Cambridge, U.K.) as a convenient mask.

**Selective Adsorption of Fluorescently-Labeled PGMA<sub>51</sub>–PBzMA<sub>100</sub> Nanoparticles onto Patterned NPPOC-Function-**

**alized Silicon Wafers.** Patterned NPPOC-functionalized silicon wafers were immersed in a 20 mM ethanolic solution of 3-formylphenylboronic acid for 2 h at 20 °C. The wafers were rinsed with ethanol and dried using a nitrogen gas stream. The phenylboronic acid-functionalized wafers were then immersed in a 0.01% w/w aqueous dispersion of fluorescently-labeled PGMA<sub>51</sub>–PBzMA<sub>100</sub> nanoparticles at either pH 4 or pH 10 for 2 h at 20 °C. Finally, each wafer was rinsed with water several times and dried gently under a nitrogen gas stream.

**Copolymer Characterization.** <sup>1</sup>H NMR Spectroscopy. All <sup>1</sup>H NMR spectra were recorded using a 400 MHz Bruker Avance-400 spectrometer using *d*<sub>4</sub>-methanol, *d*<sub>7</sub>-dimethylformamide or *d*<sub>6</sub>-dimethyl sulfoxide.

**Gel Permeation Chromatography (GPC).** The molecular weights and polydispersities of the PGMA macro-CTA and PGMA–PBzMA diblock copolymers were determined by DMF GPC at 60 °C. The GPC set-up consisted of two Polymer Laboratories PL gel 5 μm Mixed C columns connected in series to a Varian 390 LC multidetector suite (refractive index detector) and a Varian 290 LC pump injection module. The mobile phase was HPLC grade DMF containing 10 mmol LiBr with a flow rate of 1.0 mL min<sup>-1</sup>. Copolymer solutions (1.0% w/v) were prepared in DMF using DMSO as the flow rate marker. Ten near-monodisperse PMMA standards ( $M_n$  = 625 to 618 000 g mol<sup>-1</sup>) were used for calibration. Data were analyzed using Varian Cirrus GPC software (version 3.3).

**Dynamic Light Scattering (DLS).** The intensity-average hydrodynamic diameter of each batch of spherical diblock copolymer nanoparticles was determined using a Malvern Zetasizer NanoZS instrument. Aqueous dispersions (0.20% w/w) were analyzed using disposable plastic cuvettes and data were averaged over three consecutive runs.

**Transmission Electron Microscopy (TEM).** Copper/palladium TEM grids (Agar Scientific) were coated in-house to yield a thin film of amorphous carbon. The grids were then subjected to a glow discharge for 30 s to create a hydrophilic surface. Individual samples (0.20% w/w aqueous dispersion, 10.0 μL) were adsorbed onto the freshly-treated grids for 1 min and then blotted with filter paper to remove excess solution. To stain the colloidal aggregates, uranyl formate (9.0 μL of a 0.75% w/w solution) was absorbed onto the sample-loaded grid for 20 s and then carefully blotted to remove excess stain. The grids were then dried using a vacuum hose. Imaging was performed using a Philips CM100 instrument operating at 100 kV and equipped with a Gatan 1 k CCD camera.

**Optical Microscopy.** Optical microscopy images were recorded using a Motic DMBA300 digital biological microscope equipped with a built-in camera and Motic Images Plus 2.0 ML software.

**Laser Diffraction.** A Malvern Mastersizer 2000 instrument equipped with a small volume Hydro 2000SM sample dispersion unit (ca. 50 mL), a HeNe laser operating at 633 nm, and a solid-state blue laser operating at 466 nm was used to size each emulsion. The stirring rate was adjusted to 1 000 rpm in order to avoid creaming of the emulsion during analysis. After each measurement, the cell was rinsed once with ethanol, followed by two rinses with distilled water; the glass walls of the cell were carefully wiped with lens cleaning tissue to avoid cross-contamination, and the laser was aligned centrally to the detector prior to data acquisition.

**Fluorescence Microscopy.** A single droplet of a Pickering emulsion was placed on a microscope slide and viewed using an Olympus Upright Epifluorescence microscope equipped with a Hamamatsu ORCA-ER monochrome camera and Velocity software.

**Atomic Force Microscopy (AFM).** AFM studies were carried out using a Nanoscope IV Multimode Atomic Force Microscope (Veeco, Santa Barbara, CA) with a “J” scanner (0–125 μm). Silicon probes (Bruker, Germany) with average spring constants between 20 and 80 N m<sup>-1</sup> were used for tapping mode studies. Mean heights were determined for micropatterned particles.

**Table 1.** Solids Contents, Conversions, Number-Average Molecular Weights ( $M_n$ ), Polydispersities ( $M_w/M_n$ ) and Mean DLS and TEM Diameters Obtained for  $\text{PGMA}_{51}-\text{PBzMA}_x$  Diblock Copolymer Nanoparticles and the Corresponding  $\text{PGMA}_{51}$  Macro-CTA<sup>a</sup>

target composition	solids content (w/w %)	conversion <sup>b</sup> (%)	$M_n^c$	$M_w/M_n^c$	particle diameter	
					DLS (nm)	TEM (nm)
1	$\text{G}_{51}$	40	67	15 000	1.19	N/A
2	$\text{G}_{51}-\text{B}_{50}$	10	>99	19 700	1.19	28 (0.102)
3	$\text{G}_{51}-\text{B}_{75}$	10	>99	20 900	1.23	30 (0.128)
4	$\text{G}_{51}-\text{B}_{100}$	10	>99	26 900	1.22	41 (0.146)
5	$\text{G}_{51}-\text{B}_{125}$	10	>99	30 400	1.21	53 (0.245)
6	$\text{G}_{51}-\text{B}_{150}$	10	>99	34 600	1.26	55 (0.116)
7	$\text{G}_{51}-\text{B}_{175}$	10	>99	39 800	1.23	58 (0.061)
8	$\text{G}_{51}-\text{B}_{200}$	10	98	45 600	1.26	64 (0.067)
9	$\text{G}_{51}-\text{B}_{250}$	10	>99	51 100	1.19	81 (0.101)
10	$\text{G}_{51}-\text{B}_{300}$	10	>99	62 100	1.18	91 (0.053)
11	$\text{G}_{51}-\text{B}_{400}$	10	>99	77 100	1.21	113 (0.038)
12	$\text{G}_{51}-\text{B}_{500}$	10	>99	83 400	1.24	137 (0.021)
13	$\text{G}_{51}-\text{B}_{1000}$	10	>99	116 800	1.26	230 (0.017)
14	$\text{G}_{51}-\text{B}_{250}$	20	>99	52 900	1.16	78 (0.121)
15	$\text{G}_{51}-\text{B}_{250}$	30	>99	52 700	1.13	76 (0.091)
16	$\text{G}_{51}-\text{B}_{250}$	40	>99	52 700	1.13	86 (0.038)
17	$\text{G}_{51}-\text{B}_{250}$	50	>99	52 600	1.16	97 (0.095)

<sup>a</sup>The numbers in brackets refer to the DLS polydispersity of the sample. (N.B. For the sake of brevity "G" denotes PGMA and "B" denotes PBzMA.)

<sup>b</sup>Monomer conversion determined by <sup>1</sup>H NMR spectroscopy. <sup>c</sup>Determined by DMF GPC using a series of near-monodisperse poly(methyl methacrylate) calibration standards.

## RESULTS AND DISCUSSION

PGMA has been previously deployed as a reactive steric stabilizer for the synthesis of diblock copolymer nanoparticles via RAFT aqueous dispersion polymerization.<sup>36–38</sup> In particular, a PGMA macro-CTA was chain-extended with a water-miscible monomer, 2-hydroxypropyl methacrylate (HPMA). The growing water-insoluble PHPMA block led to PISA, which in turn produced a wide range of diblock copolymer morphologies, including spheres, worms, jellyfish, octopi and vesicles.<sup>39</sup> This system has been extensively studied to develop several phase diagrams which allow a particular morphology to be reproducibly targeted.<sup>36</sup>

In the present work, a PGMA macro-CTA was synthesized by RAFT solution polymerization of glycerol monomethacrylate in ethanol at 70 °C. This  $\text{PGMA}_{51}$  macro-CTA was then chain-extended with BzMA via RAFT aqueous emulsion polymerization, see Figure 1. A series of  $\text{PGMA}_{51}-\text{PBzMA}_x$  diblock copolymer nanoparticles with varying target PBzMA DPs were targeted ( $x = 50–1000$ ; see Table 1). All BzMA polymerizations proceeded to high conversions (>98% as judged by <sup>1</sup>H NMR spectroscopy; assigned NMR spectra are shown in the Supporting Information, see Figure S1).

The kinetics of the polymerization of BzMA at 70 °C was monitored using <sup>1</sup>H NMR spectroscopy for a target  $\text{PGMA}_{51}-\text{PBzMA}_{250}$  diblock composition. Sampling involved dilution of each extracted aliquot of reaction solution using *d*<sub>7</sub>-DMF, which is a good solvent for both the PGMA and PBzMA blocks (Figure 2). The effect of varying the  $\text{PGMA}_{51}$  macro-CTA/ACVA molar ratio from 3.0 to 10.0 on the rate of polymerization was also examined. As expected, the lowest macro-CTA/ACVA molar ratio led to the fastest polymerization, with >99% conversion being attained within 2 h. DMF GPC analysis of the final reaction solution indicated an  $M_n$  of 49 400 and an  $M_w/M_n$  of 1.15, which suggests that reasonably good control is still achievable under these suboptimal conditions. Higher macro-CTA/ACVA molar ratios led to

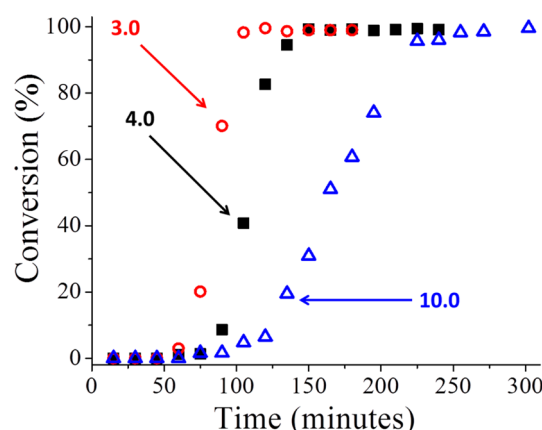


**Figure 2.** Kinetics of polymerization of BzMA at 70 °C prepared at 10% w/w solids with varying  $\text{PGMA}_{51}$  macro-CTA/ACVA molar ratios of 3.0 (red ○), 4.0 (black ■), and 10.0 (blue △). The target diblock copolymer composition in each case was  $\text{PGMA}_{51}-\text{PBzMA}_{250}$ .

significantly slower polymerizations, but both reactions nevertheless reached more than 99% conversion within 6 h at 70 °C. In each case, the final polydispersity of the  $\text{PGMA}_{51}-\text{PBzMA}_{250}$  diblock copolymer chains was below 1.20.

DMF GPC analysis also indicated high blocking efficiencies, since there was minimal contamination of the diblock copolymer chains with unreacted  $\text{PGMA}_{51}$  macro-CTA (see Figure 3). A monotonic increase in diblock copolymer  $M_n$  was observed as higher PBzMA DPs were targeted. Remarkably, polydispersities remained below 1.30 even when targeting highly asymmetric diblock compositions such as  $\text{PGMA}_{51}-\text{PBzMA}_{1000}$  (see Table 1). For this particular copolymer composition, there is some apparent tailing to higher molecular weight. Given that the BzMA monomer is unlikely to contain dimethacrylate impurities, this may indicate some low level of termination by combination for this methacrylic formulation.

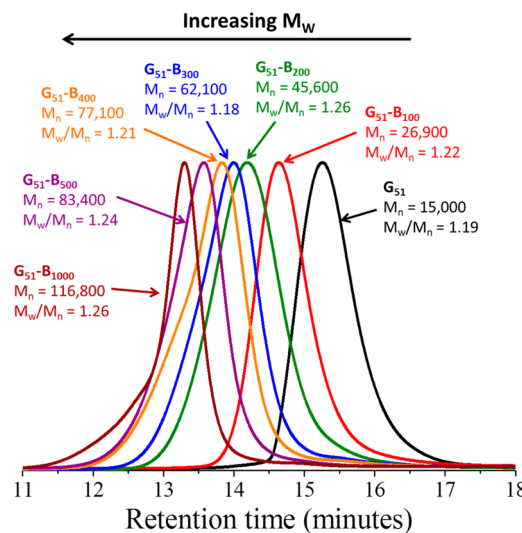


**Figure 3.** DMF GPC curves for  $\text{PGMA}_{51}-\text{PBzMA}_x$  diblock copolymers prepared at 10% w/w solids via RAFT aqueous emulsion polymerization of BzMA at 70 °C, where  $x = 100, 200, 300, 400, 500$ , or 1000. Molecular weight data are expressed relative to a series of near-monodisperse poly(methyl methacrylate) calibration standards (N.B. “G” denotes PGMA and “B” denotes PBzMA).

DLS was used to characterize dilute aqueous dispersions of  $\text{PGMA}_{51}-\text{PBzMA}_x$  nanoparticles. For a fixed  $\text{PGMA}_{51}$  macro-CTA, targeting higher PBzMA DPs proved to be a highly convenient means of controlling the particle size (see Table 1 and Figure 4). For example,  $\text{PGMA}_{51}-\text{PBzMA}_{50}$  self-assembled to form spherical particles with a mean hydrodynamic diameter of 28 nm, while  $\text{PGMA}_{51}-\text{PBzMA}_{1000}$  formed particles of around 230 nm. A monotonic relationship was observed between the DLS diameter and the target DP of the core-forming block over a wide particle size range. This

approximately linear correlation was also supported by TEM studies (Figure 4c). Moreover, relatively narrow particle size distributions were achieved in each case. This can be fitted to a power law of the form  $d = kN^\alpha$ , where  $d$  is the core diameter,  $N$  is the mean DP of the hydrophobic PBzMA block,  $k$  is a constant that depends on the Flory–Huggins parameter and  $N$  scales with an exponent  $\alpha$ .<sup>40</sup> From this the PGMA–PBzMA spherical particles have  $\alpha = 0.73$  as measured by DLS and  $\alpha = 0.78$  as measured by TEM. This is consistent with the PGMA–PHPMA spherical particles and suggests that the PBzMA chains are neither fully stretched nor collapsed.<sup>41</sup>

It is also worth emphasizing that these diblock copolymer nanoparticles invariably possess a rather more well-defined spherical morphology than the PGMA–PHPMA diblock copolymer nanoparticles prepared via RAFT aqueous dispersion polymerization.<sup>36,37,42</sup> However, unlike the latter formulation, it was not possible to access either worm or vesicular morphologies, even though a wide range of diblock compositions and copolymer concentrations were explored. In view of the worm and vesicle morphologies observed in RAFT aqueous emulsion polymerization studies reported by Charleux and co-workers,<sup>17,22,25</sup> there seems to be no intrinsic reason for the morphological limitations observed in the present study. For highly asymmetric diblock copolymers such as  $\text{PGMA}_{51}-\text{PBzMA}_{1000}$ , the elegant studies of diblock copolymer vesicles conducted by Eisenberg’s group<sup>43</sup> suggest that the observed spherical particles must represent a kinetically-trapped morphology, rather than the equilibrium morphology. In the case of RAFT aqueous dispersion polymerization, monomer plasticization of the core-forming block is believed to be important, if not essential, for mediating the evolution in block copolymer morphology from spheres to worms to vesicles that is observed when targeting asymmetric diblock copolymers.<sup>36</sup> For the present RAFT aqueous emulsion polymerization, it is conceivable that diffusion of the water-immiscible BzMA monomer through the aqueous phase occurs too slowly on

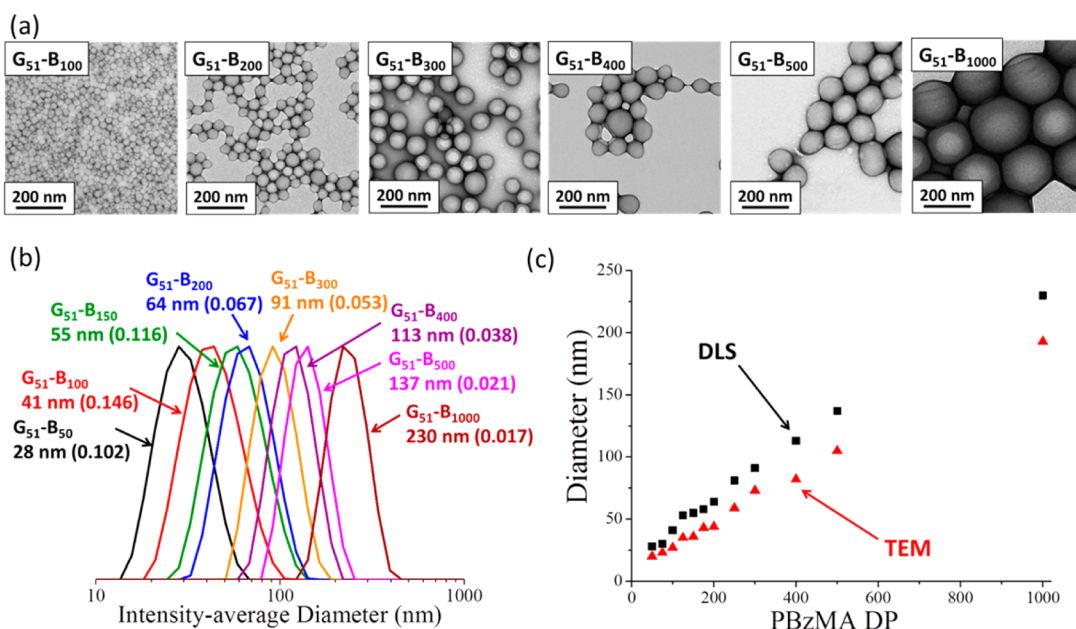


**Figure 4.**  $\text{PGMA}_{51}-\text{PBzMA}_x$  diblock copolymers prepared at 10% w/w solids via RAFT aqueous emulsion polymerization of BzMA at 70 °C: (a) TEM images showing well-defined spherical nanoparticles, (b) the corresponding DLS intensity-average size distributions, and (c) a plot of mean particle diameter vs mean degree of polymerization of the PBzMA core-forming block (N.B. for the sake of brevity ‘G’ denotes PGMA and ‘B’ denotes PBzMA).

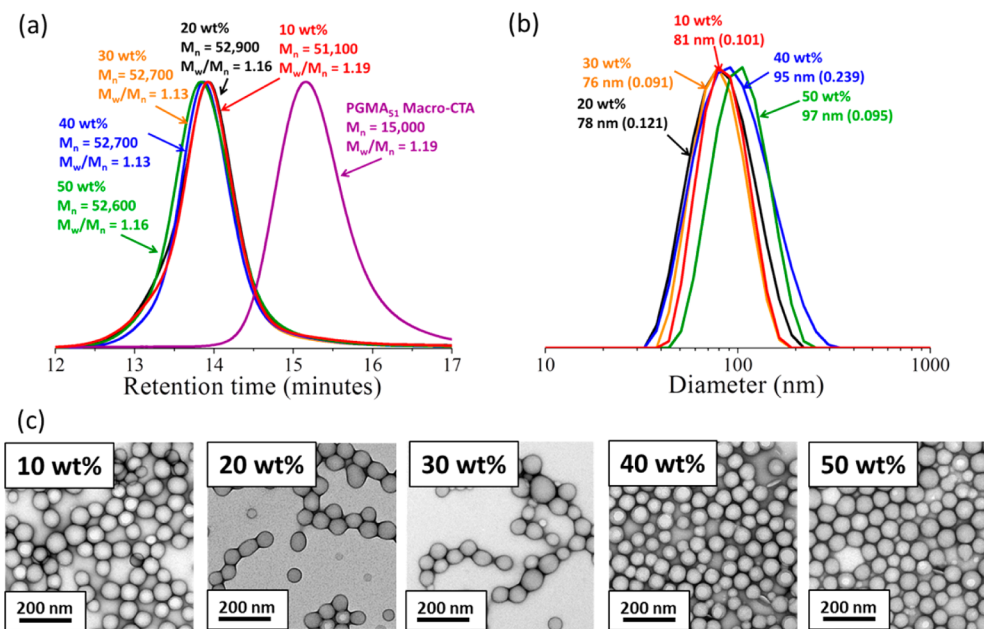


**Figure 5.** PGMA<sub>51</sub>-PBzMA<sub>250</sub> spherical nanoparticles prepared at either 10, 20, 30, 40 or 50% w/w solids via RAFT aqueous emulsion polymerization of benzyl methacrylate using a PGMA<sub>51</sub> macro-CTA at 70 °C: (a) DMF GPC curves obtained for PGMA<sub>51</sub> macro-CTA and PGMA<sub>51</sub>-PBzMA<sub>250</sub> diblock copolymers prepared at solids contents ranging from 10 to 50% w/w; (b) the corresponding DLS intensity-average size distributions and polydispersities determined for these five dispersions; (c) representative TEM images obtained for the same set of five PGMA<sub>51</sub>-PBzMA<sub>250</sub> dispersions prepared at 10, 20, 30, 40, or 50% w/w solids; a reasonably well-defined spherical morphology is obtained in each case.

the time scale of the polymerization to provide sufficient plasticization of the growing PBzMA blocks. However, such a mass transport problem might also be expected for the styrene-based formulations reported by Charleux and co-workers, yet this is clearly not the case.<sup>15,20,23</sup> This fundamental aspect clearly warrants further studies and serves to illustrate our incomplete understanding of RAFT-mediated PISA formulations.

Charleux and co-workers have recently reported that the RAFT emulsion polymerization of styrene enables the synthesis of diblock copolymer nanoparticles with worm-like and vesicular morphologies, as well as the more common spherical morphology.<sup>22,25</sup> For many formulations, utilizing a relatively short stabilizer block and targeting a sufficiently high DP for the core-forming block is sufficient to enable the particle morphology to evolve from spherical particles to worm-like micelles/rods to vesicles during polymerization.<sup>25</sup> Similar observations have been reported for RAFT aqueous dispersion polymerizations based on various water-soluble stabilizer blocks coupled with a PHPMA core-forming block.<sup>36,39,41,44,45</sup> For these latter formulations, it has been shown that the copolymer concentration can also profoundly affect the particle morphology, with copolymer nanoparticles prepared at relatively low concentrations (e.g., 10% w/w solids) forming kinetically-trapped spheres.<sup>36</sup> Thus a series of PGMA<sub>18</sub>-PBzMA<sub>x</sub> diblock copolymers were synthesized via RAFT aqueous emulsion polymerization at 20% w/w solids to explore the possibility of accessing worm and vesicular morphologies. <sup>1</sup>H NMR spectroscopy studies confirmed that high BzMA conversions ( $\geq 99\%$ ) were obtained for all such syntheses (see Supporting Information, Table S1). However, DLS and TEM studies confirmed the presence of only spherical particles. PBzMA has been utilized as the core-forming block for RAFT dispersion polymerizations conducted in alcohol<sup>46</sup> and *n*-alkanes.<sup>47</sup> In each case the full range of copolymer morphologies (e.g., spheres,

worms or vesicles) can be obtained. Hence the limitation to spheres observed for the current RAFT aqueous emulsion polymerization does not appear to be an intrinsic problem associated with the selection of PBzMA as a core-forming block.

In the literature, RAFT PISA syntheses conducted via aqueous emulsion or aqueous dispersion polymerization are typically performed at 10–30% solids.<sup>22,25,29,36,37,45–48</sup> However, commercial latexes are normally synthesized at up to 50% solids using conventional free radical emulsion polymerization under monomer-starved conditions.<sup>2</sup> In the present work, we wished to examine whether our RAFT aqueous emulsion polymerization formulation could be performed successfully under such conditions. Thus, a series of PGMA<sub>51</sub>-PBzMA<sub>250</sub> syntheses were set up at total solids contents varying from 10 to 50% w/w. More than 99% BzMA conversion was achieved in each case, as judged by <sup>1</sup>H NMR spectroscopy studies of the final reaction solutions (see entries 14–17 in Table 1). DMF GPC analyses (see Figure 5a) indicated high blocking efficiencies and low final polydispersities ( $M_w/M_n < 1.20$ ). Moreover, almost identical PMMA-equivalent  $M_n$  values of approximately 52 000 were obtained in each case, as expected for a fixed target diblock copolymer composition. TEM analyses of this series of PGMA<sub>51</sub>-PBzMA<sub>250</sub> nanoparticles confirmed that well-defined spherical nanoparticles were obtained in each case. Mean number-average particle diameters (with at least 100 particles being counted in each case) for PGMA<sub>51</sub>-PBzMA<sub>250</sub> diblock copolymers prepared at 10% and 50% were calculated to be  $55 \pm 8$  nm and  $57 \pm 16$  nm, respectively. Thus, there is no significant variation in particle size when conducting such syntheses at high solids. However, DLS studies of the same series of nanoparticles indicated modest size differences, with slightly larger apparent particle diameters being obtained for polymerizations conducted in more concentrated media (see Figure 5b). DLS reports an

**Table 2. DLS Particle Diameter (nm) Determined Before and After Either the Addition of 0.25 M MgSO<sub>4</sub> or a Single Freeze–Thaw Cycle (at –21 °C)<sup>a</sup>**

target composition	particle diameter	addition of 0.25 M MgSO <sub>4</sub>	effect of one freeze–thaw cycle	stabilizer content (w/w %)	$\Gamma^b$ (mg m <sup>-2</sup> )
G <sub>51</sub> –B <sub>100</sub>	41 (0.146)	48 (0.137)	44 (0.167)	13.5	2.46
G <sub>51</sub> –B <sub>175</sub>	58 (0.061)	67 (0.048)	60 (0.125)	21.2	2.22
G <sub>51</sub> –B <sub>250</sub>	81 (0.101)	89 (0.127)	83 (0.137)	15.9	1.99

<sup>a</sup>The numbers in brackets refer to the DLS polydispersity of the sample (N.B. For the sake of brevity “G” denotes PGMA and “B” denotes PBzMA).

<sup>b</sup>Adsorbed amount of PGMA<sub>51</sub> stabilizer (in mg) per unit surface area of nanoparticles.

intensity-average diameter, thus for particle size distributions of finite width this technique is expected to oversize relative to the number-average diameter reported by TEM. In addition, the solvated PGMA stabilizer chains will also increase the hydrodynamic diameter detected by DLS but make a negligible contribution to the TEM diameter (since the stabilizer chains collapse under the ultrahigh vacuum conditions required for electron microscopy). Thus, in principle the difference between the DLS and TEM diameters for a given sample of diblock copolymer nanoparticles should provide an upper limit estimate for the stabilizer layer thickness.<sup>49</sup> However, the observed apparent increase in DLS diameter for polymerizations conducted at higher solids may also indicate some incipient flocculation. This hypothesis is supported by the paste-like consistency observed for dispersions prepared at 50% solids (see Figure S2 in the Supporting Information). It seems likely that the PGMA stabilizer is unable to offset the ever-present weak attractive interparticle interactions in this case. In contrast, free-flowing fluids were obtained for sterically-stabilized diblock copolymer nanoparticles prepared at 10–40% solids.

The colloidal stabilities of three nanoparticle dispersions (PGMA<sub>51</sub>–PBzMA<sub>100</sub>, PGMA<sub>51</sub>–PBzMA<sub>175</sub> and PGMA<sub>51</sub>–PBzMA<sub>250</sub>) were assessed by (i) conducting a freeze–thaw cycle at –21 °C and (ii) addition of salt (0.25 M MgSO<sub>4</sub>). In such studies, DLS is an appropriate characterization technique for assessing any increase in the degree of flocculation, since this technique is very sensitive to a relatively small (apparent) increase in particle size. However, in each case only a minimal increase (<10 nm) in the mean particle diameter was observed (see Table 2). Such observations provide good evidence for the robust steric stabilization conferred by the highly hydrophilic PGMA block.

Thompson et al. reported that PGMA-stabilized polystyrene latexes of around ~90 nm diameter can be readily prepared by conducting the aqueous emulsion polymerization of styrene in the presence of a well-defined PGMA<sub>50</sub> macromonomer (previously prepared via ATRP using a tertiary amine-functionalized ATRP initiator).<sup>50</sup> Although these latexes proved to be interesting Pickering emulsifiers (see below), such syntheses suffered from substantially incomplete monomer conversions (< 70%).<sup>50</sup> Thus the RAFT aqueous emulsion polymerization formulation reported in the present study appears to be a superior route for the efficient preparation of well-defined PGMA-stabilized nanoparticles.

Three PGMA<sub>51</sub>–PBzMA<sub>x</sub> syntheses ( $x = 100, 175$  or  $250$ ) were scaled up and the resulting spherical particles were evaluated as putative Pickering emulsifiers. An aqueous dispersion of PGMA<sub>51</sub>–PBzMA<sub>250</sub> diblock copolymer nanoparticles prepared at 10% w/w solids (entry 9 in Table 1; mean TEM diameter = 55 nm) was serially diluted to prepare dispersions ranging from 2.50 to 0.0675% w/w. A 2.0 mL aliquot of each dispersion was homogenized with an equal

volume of sunflower oil at 12 000 rpm for 2 min to form a series of oil-in-water emulsions. Figure 6a shows laser diffraction studies for the spherical sunflower oil droplets obtained at various copolymer concentrations. Despite the relatively broad droplet size distribution, a gradual reduction in the mean emulsion droplet diameter is observed at higher copolymer concentrations. This is confirmed by optical microscopy images (see Figure S3 in the Supporting Information) and similar effects have been observed for many types of Pickering emulsifiers reported by various research groups.<sup>50–52</sup> Allowing these emulsions to stand overnight at 20 °C led to creaming of the oil droplets. The underlying aqueous phase was weakly turbid rather than transparent, which suggested that not all of the nanoparticles were adsorbed onto the oil droplets. Similar observations have been reported for other latex-based Pickering emulsifiers.<sup>53–57</sup> In contrast, Thompson et al. reported that PGMA-stabilized polystyrene latexes (prepared by conducting the aqueous emulsion polymerization of styrene in the presence of well-defined PGMA<sub>50</sub> macromonomers) adsorbed very efficiently onto various types of oil droplets.<sup>50</sup> Given that the surface of the block copolymer nanoparticles utilized in the present work is also PGMA-rich, this discrepancy is perhaps surprising. One explanation may be that the PGMA–PBzMA nanoparticles used in the present work are significantly smaller than the ~90 nm diameter latexes utilized by Thompson et al.<sup>58</sup> According to Binks, smaller particles are much less strongly adsorbed than larger particles when deployed as Pickering emulsifiers.<sup>59</sup> Moreover, given that the blocking efficiency of the PGMA<sub>51</sub> macro-CTA in the synthesis of the PGMA<sub>51</sub>–PBzMA<sub>250</sub> nanoparticles is relatively high (>90%), then the surface concentration of the highly hydrophilic PGMA chains is likely to be significantly higher than that of the PGMA-stabilized polystyrene latexes previously reported by Thompson et al.<sup>50</sup> <sup>1</sup>H NMR analysis of the dried nanoparticles allowed the PGMA content of the particles to be calculated (13.5–21.2% w/w). Assuming that all the PGMA chains are located at the surface of the nanoparticles, this corresponds to an adsorbed amount,  $\Gamma$ , of 2.0–2.5 mg m<sup>-2</sup> (see Table 2). This is a little higher than the 1.8 mg m<sup>-2</sup> reported by Thompson et al. for a PGMA<sub>50</sub> macromonomer,<sup>58</sup> which probably reflects the greater blocking efficiency of the PGMA<sub>51</sub> macro-CTA compared to the macromonomer grafting efficiency. This higher surface concentration of PGMA chains is expected to lower the particle contact angle (or particle wettability), which in turn should lead to weaker interfacial adsorption. Furthermore, DLS characterization of the non-adsorbed PGMA<sub>51</sub>–PBzMA<sub>250</sub> nanoparticles remaining in the underlying aqueous phase indicated that significant flocculation had occurred during high-shear homogenization. This problem has not been previously reported for latex-based Pickering emulsifiers<sup>53–57</sup> and probably warrants further investigation. Unfortunately, this unexpected particle aggregation also prevented the adsorption

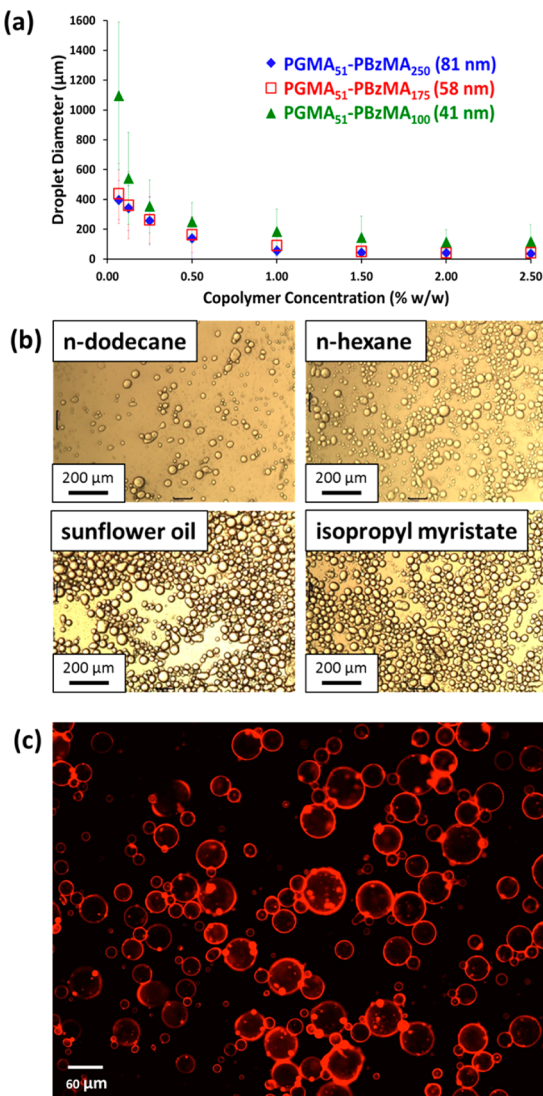


**Figure 6.** (a) Concentration dependence of mean diameter of sunflower oil droplets (as determined by laser diffraction) prepared using PGMA<sub>51</sub>-PBzMA<sub>x</sub> nanoparticles as the sole emulsifier, where  $x = 100, 175$ , or  $250$ . Error bars represent the standard deviation of the volume-average droplet diameters, rather than the experimental uncertainty. (b) Representative optical microscopy images obtained for oil-in-water Pickering emulsions prepared using PGMA<sub>51</sub>-PBzMA<sub>250</sub> nanoparticles as the sole emulsifier at  $1.00\%$  w/w using either *n*-dodecane, *n*-hexane, sunflower oil, or isopropyl myristate as the oil phase. Scale bar =  $200\text{ }\mu\text{m}$  in each case. (c) Fluorescence microscopy image of sunflower-in-water Pickering emulsion droplets prepared using  $0.50\%$  w/w PGMA<sub>51</sub>-PBzMA<sub>100</sub> nanoparticles labeled with rhodamine B isothiocyanate.

efficiency of the nanoparticles being determined by turbidimetry, as previously reported by Thompson et al. in the context of cross-linked vesicle-based Pickering emulsifiers.<sup>56</sup> Thus an alternative approach was employed whereby, after creaming of the emulsion droplets had occurred on standing, a known amount of the underlying aqueous phase was dried at  $70\text{ }^{\circ}\text{C}$  for 2 days. The dry residues were then redissolved in a fixed known volume of DMF, which is a good solvent for both the PGMA and the PBzMA blocks. Molecular dissolution of the diblock copolymer in this solvent eliminated the flocculation problem and allowed the adsorption efficiency to be calculated via UV spectroscopy. A linear calibration plot at  $268\text{ nm}$  (correspond-

ing to the aromatic benzyl chromophore in the PBzMA block) was constructed to determine the amount of non-adsorbed particles remaining in the aqueous phase (see Figure S4 in the Supporting Information). This supernatant depletion assay was used to assess the nanoparticle adsorption efficiency for Pickering emulsions prepared using PGMA<sub>51</sub>-PBzMA<sub>250</sub> particles. A maximum adsorption efficiency of  $80\%$  was calculated when emulsification was performed using a copolymer concentration of  $0.0675\%$  w/w. A gradual reduction in adsorption efficiency was observed with increasing nanoparticle concentration, with only  $22\%$  efficiency being obtained for the highest nanoparticle concentration investigated in this work ( $2.50\%$  w/w).

The same emulsification protocol was also used to prepare oil-in-water Pickering emulsions using either PGMA<sub>51</sub>-PBzMA<sub>100</sub> or PGMA<sub>51</sub>-PBzMA<sub>175</sub> nanoparticles. Again, the variation of droplet diameter with nanoparticle concentration was determined by laser diffraction (Figure 6a). Finer droplets were obtained when using higher nanoparticle concentrations, up to a limiting copolymer concentration of around  $1.50\%$  w/w. At lower nanoparticle concentrations, larger volume-average droplet diameters were observed when using the smallest nanoparticles (PGMA<sub>51</sub>-PBzMA<sub>100</sub>;  $41\text{ nm}$  diameter as judged by DLS). It has been previously shown that the energy of detachment of a particle at the oil–water interface increases with particle size.<sup>59</sup> Thus, relatively small particles require significantly less energy to be desorbed from the oil/water interface, which results in larger, less stable Pickering emulsions being obtained at lower copolymer concentrations.

The PGMA<sub>51</sub>-PBzMA<sub>250</sub> nanoparticles were also utilized to prepare Pickering emulsions using three additional model oils: *n*-dodecane, *n*-hexane or isopropyl myristate. In each case, stable oil-in-water Pickering emulsions were obtained. The optical microscopy images shown in Figure 6b were recorded when using a  $1.00\%$  w/w aqueous PGMA<sub>51</sub>-PBzMA<sub>250</sub> dispersion as a Pickering emulsifier. Fluorescence microscopy studies of a Pickering emulsion prepared using  $0.5\%$  w/w PGMA<sub>51</sub>-PBzMA<sub>100</sub> tagged with rhodamine B isothiocyanate (see Experimental Section for further details) confirmed that these fluorescently-labeled nanoparticles were indeed located at the oil droplet surface, as expected (see Figure 6c).<sup>60</sup>

Phenylboronic acid derivatives have been reported to form a 1:1 cyclic boronate ester complex with PGMA in aqueous alkaline solution.<sup>33,34</sup> More specifically, this chemistry was exploited to achieve pH-modulated binding of PGMA-stabilized polystyrene latexes onto cellulose fibers.<sup>33</sup> Latex adsorption was observed at pH  $10.5$ , with substantial desorption occurring at pH  $4$  on washing with dilute acid. This work was subsequently extended to demonstrate specific binding of the same PGMA-stabilized latexes onto both planar and colloidal silica substrates.<sup>35</sup>

In the present work, selective binding of PGMA<sub>51</sub>-PBzMA<sub>100</sub> nanoparticles onto a micropatterned planar silicon wafer functionalized with phenylboronic acid groups was examined (see Figure 7). This model surface was prepared by exposing selected areas of NPPOC-treated silicon wafers to UV irradiation at  $325\text{ nm}$  using a patterned photomask, as previously described by Leggett and co-workers.<sup>61</sup> The exposed primary amine surface groups were then reacted with excess 3-formylphenylboronic acid to form imine linkages via Schiff base chemistry.<sup>62,63</sup> Such phenylboronic acid-functionalized planar silicon wafers were then immersed in a  $0.01\%$  w/w aqueous dispersion of PGMA<sub>51</sub>-PBzMA<sub>100</sub> nanoparticles for  $2\text{ h}$   $20\text{ }^{\circ}\text{C}$

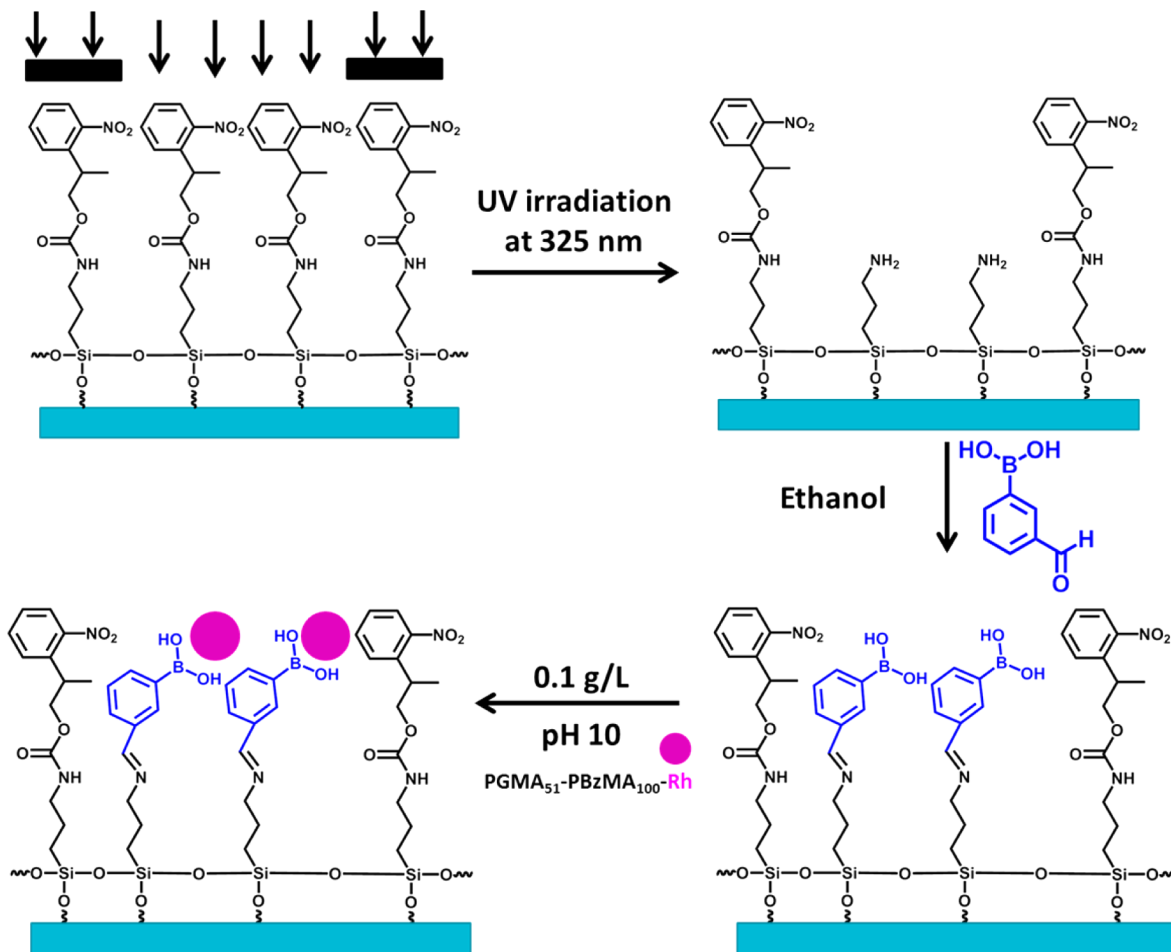


**Figure 7.** Schematic representation of a micropatterned NPPOC-functionalized planar silicon wafer prepared via UV irradiation ( $\lambda = 325 \text{ nm}$ ) using a photomask. The exposed surface amine groups were reacted with excess 3-formylphenylboronic acid to enable the pH-modulated selective binding of rhodamine B-labeled PGMA<sub>51</sub>-PBzMA<sub>100</sub> nanoparticles to the planar silicon wafer.

at either pH 4 or pH 10, followed by imaging via atomic force microscopy (AFM). Figure 8a depicts a friction force image recorded for the micropatterned phenylboronic acid-functionalized planar silicon wafer prior to exposure to PGMA<sub>51</sub>-PBzMA<sub>100</sub> nanoparticles. Minimal nanoparticle adsorption was observed on the micropatterned silicon wafer at pH 4, because this solution pH is below the  $pK_a$  of approximately 8 for phenylboronic acid (Figure 8b).<sup>64</sup> In contrast, selective nanoparticle adsorption occurs at pH 10, see Figure 8c. Surprisingly, extensive washing of this nanoparticle-coated surface with a mildly acidic solution (pH 4) only led to partial nanoparticle desorption (data not shown), whereas Pelton and co-workers reported rather more efficient desorption for PGMA-stabilized polystyrene latexes coated onto cellulose fibers using the same phenylboronic acid chemistry.<sup>33</sup> To confirm that surface binding was indeed the result of the cis-diol chemistry of the PGMA stabilizer chains, a control experiment was conducted using poly(ethylene glycol)<sub>113</sub>-PBzMA<sub>200</sub> spherical nanoparticles of 122 nm diameter prepared via RAFT emulsion polymerization (see Supporting Information for synthesis details). These latter nanoparticles possess no cis-diol functionality and hence were unable to bind selectively to the micropatterned surface at pH 10; see Figure 8d.

## CONCLUSIONS

We report a rare example of a RAFT emulsion polymerization formulation using a *non-ionic* block as the steric stabilizer. A water-soluble PGMA macro-CTA is readily chain-extended using BzMA monomer to form a series of PGMA-PBzMA diblock copolymer nanoparticles via polymerization-induced self-assembly. However, unlike the well-documented RAFT aqueous dispersion polymerization of 2-hydroxypropyl methacrylate using a similar PGMA macro-CTA, only spherical morphologies could be obtained, despite exploring a wide range of formulations. The reason for this fundamental difference is unclear at present. However, it does not seem to be an intrinsic problem associated with the core-forming block, because a full range of copolymer morphologies (spheres, worms and vesicles) has been reported for PBzMA-based diblock copolymer nanoparticles in both alcoholic media and *n*-alkanes. Judicious variation of the PGMA<sub>51</sub>-PBzMA<sub>x</sub> diblock composition enabled the mean diameter of the spherical particles to be controlled over a relatively wide range, from 20 to  $\sim 200$  nm as judged by both DLS and TEM. Moreover, well-defined spherical PGMA<sub>51</sub>-PBzMA<sub>250</sub> particles can be efficiently prepared at up to 50% solids in the absence of any surfactant, with minimal differences in particle diameter, molecular weight, polydispersity and blocking efficiency compared to nanoparticles synthesized at lower copolymer concentrations.

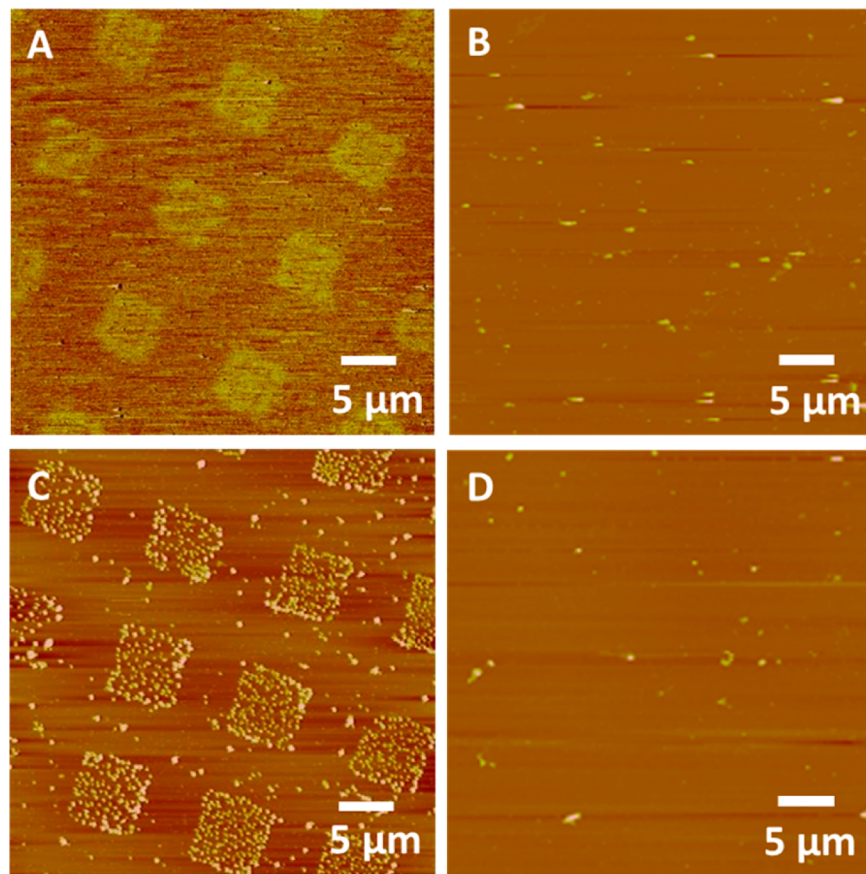


**Figure 8.** Atomic force microscopy (AFM) images obtained for 46 nm diameter PGMA<sub>51</sub>-PBzMA<sub>100</sub> nanoparticles adsorbed from aqueous solution at 20 °C onto a micropatterned phenylboronic acid-functionalized planar silicon wafer. (a) Friction force image recorded for the patterned NPPOC silicon wafer prior to exposure to any nanoparticles. (b) Height image recorded at pH 4, confirming that minimal PGMA<sub>51</sub>-PBzMA<sub>100</sub> nanoparticle binding occurs under these conditions. (c) Height image recorded for PGMA<sub>51</sub>-PBzMA<sub>100</sub> nanoparticles at pH 10, showing selective nanoparticle adsorption via complexation between the cis-diol groups on the PGMA stabilizer chains with the phenylboronic acid groups on the wafer surface. (d) Height image recorded for the attempted selective adsorption of 122 nm diameter PEG<sub>113</sub>-PBzMA<sub>200</sub> nanoparticles at pH 10 onto the same micropatterned planar silicon wafer. In this case selective adsorption cannot occur, since the latter nanoparticles lack the cis-diol functionality required to bind to the wafer surface. The height images shown in (b)–(d) were obtained using tapping mode AFM. For the friction force image shown in (a), a silicon nitride nanoprobe was utilized with a nominal spring constant of 0.12 N m<sup>-1</sup> and a tip radius of 20–60 nm.

Three examples of PGMA<sub>51</sub>-PBzMA<sub>x</sub> diblock copolymer nanoparticles (where  $x = 100, 175$  or  $250$ ) were used to prepare a series of Pickering emulsions for four model oils. Polydisperse emulsion droplets with good long-term resistance toward droplet coalescence were obtained in each case. A monotonic reduction in the mean diameter of sunflower droplets from 1100 to 50  $\mu\text{m}$  was observed via laser diffraction studies on increasing the PGMA<sub>51</sub>-PBzMA<sub>250</sub> nanoparticle concentration from 0.0675% to 2.50% w/w.

The cis-diol functionality on the PGMA stabilizer chain was exploited to demonstrate pH-modulated binding of PGMA<sub>51</sub>-PBzMA<sub>100</sub> nanoparticles onto a model phenylboronic acid-functionalized micropatterned planar substrate. Nanoparticle adsorption occurred at pH 10, whereas little or no binding was observed at pH 4. However, only partial nanoparticle desorption was achieved on lowering the pH from 10 to 4.

PGMA<sub>18</sub>-PBzMA<sub>x</sub>, optical microscopy images of PGMA<sub>51</sub>-PBzMA<sub>250</sub>-stabilized Pickering emulsion droplets, and synthesis details for the PEG<sub>113</sub>-PBzMA<sub>200</sub> nanoparticles. This material is available free of charge via the Internet at <http://pubs.acs.org>.

## ■ AUTHOR INFORMATION

### Corresponding Author

\*(S.P.A.) E-mail: s.p.armes@sheffield.ac.uk.

### Notes

The authors declare no competing financial interest.

## ■ ACKNOWLEDGMENTS

EPSRC is thanked for a Ph.D. studentship and a Programme Grant (EP/I012060/1). Ashland Specialty Ingredients (Bridgewater, NJ) is thanked for CASE support of this Ph.D. project and for permission to publish this work.

## ■ REFERENCES

- (1) Lovell, P. A.; El-Aasser, M. S. *Emulsion polymerization and emulsion polymers*; Wiley: New York, 1997.
- (2) Urban, D.; Takamura, K. *Polymer dispersions and their industrial applications*; Wiley-VCH: New York, 2002.
- (3) Guyot, A. *Curr. Opin. Colloid Interface Sci.* **1996**, *1*, 580.

## ■ ASSOCIATED CONTENT

### Supporting Information

Assigned <sup>1</sup>H NMR spectra for the PGMA<sub>51</sub> macro-CTA and PGMA<sub>51</sub>-PBzMA<sub>100</sub> digital photographs and TEM images of PGMA<sub>51</sub>-PBzMA<sub>250</sub> prepared at 10% and 50% w/w solids, summary of conversions, GPC data and particle size data for

- (4) Hawker, C. J. *J. Am. Chem. Soc.* **1994**, *116*, 11185.  
(5) Benoit, D.; Chaplinski, V.; Braslau, R.; Hawker, C. J. *J. Am. Chem. Soc.* **1999**, *121*, 3904.  
(6) Wang, J.-S.; Matyjaszewski, K. *Macromolecules* **1995**, *28*, 7901.  
(7) Chieffari, J.; Chong, Y.; Ercole, F.; Krstina, J.; Jeffery, J.; Le, T. P.; Mayadunne, R. T.; Meijis, G. F.; Moad, C. L.; Moad, G. *Macromolecules* **1998**, *31*, 5559.  
(8) Charleux, B.; Delaittre, G.; Rieger, J.; D'Agosto, F. *Macromolecules* **2012**, *45*, 6753.  
(9) Cunningham, M. F. *Prog. Polym. Sci.* **2008**, *33*, 365.  
(10) Monteiro, M. J.; Hodgson, M.; De Brouwer, H. *J. Polym. Sci., Part A: Polym. Chem.* **2000**, *38*, 3864.  
(11) Prescott, S. W.; Ballard, M. J.; Rizzardo, E.; Gilbert, R. G. *Macromolecules* **2002**, *35*, 5417.  
(12) Ferguson, C. J.; Hughes, R. J.; Pham, B. T. T.; Hawkett, B. S.; Gilbert, R. G.; Serelis, A. K.; Such, C. H. *Macromolecules* **2002**, *35*, 9243.  
(13) Ferguson, C. J.; Hughes, R. J.; Nguyen, D.; Pham, B. T. T.; Gilbert, R. G.; Serelis, A. K.; Such, C. H.; Hawkett, B. S. *Macromolecules* **2005**, *38*, 2191.  
(14) Sprong, E.; Leswin, J. S. K.; Lamb, D. J.; Ferguson, C. J.; Hawkett, B. S.; Pham, B. T. T.; Nguyen, D.; Such, C. H.; Serelis, A. K.; Gilbert, R. G. *Macromol. Symp.* **2006**, *231*, 84.  
(15) Ganeva, D. E.; Sprong, E.; de Bruyn, H.; Warr, G. G.; Such, C. H.; Hawkett, B. S. *Macromolecules* **2007**, *40*, 6181.  
(16) Boissé, S.; Rieger, J.; Belal, K.; Di-Cicco, A.; Beaunier, P.; Li, M.-H.; Charleux, B. *Chem. Commun.* **2010**, *46*, 1950.  
(17) Boissé, S.; Rieger, J.; Pembouong, G.; Beaunier, P.; Charleux, B. *J. Polym. Sci., Part A: Polym. Chem.* **2011**, *49*, 3346.  
(18) Chaduc, I.; Crepet, A.; Boyron, O.; Charleux, B.; D'Agosto, F.; Lansalot, M. *Macromolecules* **2013**, *46*, 6013.  
(19) Manguian, M.; Save, M.; Charleux, B. *Macromol. Rapid Commun.* **2006**, *27*, 399.  
(20) Rieger, J.; Zhang, W.; Stoffelbach, F.; Charleux, B. *Macromolecules* **2010**, *43*, 6302.  
(21) Chaduc, I.; Zhang, W.; Rieger, J.; Lansalot, M.; D'Agosto, F.; Charleux, B. *Macromol. Rapid Commun.* **2011**, *32*, 1270.  
(22) Zhang, X.; Boissé, S.; Zhang, W.; Beaunier, P.; D'Agosto, F.; Rieger, J.; Charleux, B. *Macromolecules* **2011**, *44*, 4149.  
(23) Rieger, J.; Osterwinter, G.; Bui, C.; Stoffelbach, F.; Charleux, B. *Macromolecules* **2009**, *42*, 5518.  
(24) Zhang, X.; Rieger, J.; Charleux, B. *Polym. Chem.* **2012**, *3*, 1502.  
(25) Zhang, W.; D'Agosto, F.; Boyron, O.; Rieger, J.; Charleux, B. *Macromolecules* **2012**, *45*, 4075.  
(26) Zhang, W.; D'Agosto, F.; Boyron, O.; Rieger, J.; Charleux, B. *Macromolecules* **2011**, *44*, 7584.  
(27) Chaduc, I.; Girod, M.; Antoine, R.; Charleux, B.; D'Agosto, F.; Lansalot, M. *Macromolecules* **2012**, *45*, 5881.  
(28) Zhang, W.; D'Agosto, F.; Dugas, P.-Y.; Rieger, J.; Charleux, B. *Polymer* **2013**, *54*, 2011.  
(29) Rieger, J.; Stoffelbach, F.; Bui, C.; Alaimo, D.; Jérôme, C.; Charleux, B. *Macromolecules* **2008**, *41*, 4065.  
(30) Velasquez, E.; Rieger, J.; Stoffelbach, F.; Charleux, B.; D'Agosto, F.; Lansalot, M.; Dufils, P.-E.; Vinas, J. *Polymer* **2013**, *54*, 6547.  
(31) Minami, H.; Shimomura, K.; Suzuki, T.; Sakashita, K.; Noda, T. *Macromolecules* **2013**, *47*, 130.  
(32) Xu, J.; Xiao, X.; Zhang, Y.; Zhang, W.; Sun, P. *J. Polym. Sci., Part A: Polym. Chem.* **2013**, *51*, 1147.  
(33) Zhang, D.; Thompson, K. L.; Pelton, R.; Armes, S. P. *Langmuir* **2010**, *26*, 17237.  
(34) Pelton, R.; Zhang, D.; Thompson, K. L.; Armes, S. P. *Langmuir* **2011**, *27*, 2118.  
(35) Pelton, R.; Cui, Y.; Zhang, D.; Chen, Y.; Thompson, K. L.; Armes, S. P.; Brook, M. A. *Langmuir* **2013**, *29*, 594.  
(36) Blanazs, A.; Ryan, A. J.; Armes, S. P. *Macromolecules* **2012**, *45*, 5099.  
(37) Blanazs, A.; Verber, R.; Mykhaylyk, O. O.; Ryan, A. J.; Heath, J. Z.; Douglas, C. W. L.; Armes, S. P. *J. Am. Chem. Soc.* **2012**, *134*, 9741.  
(38) Chambon, P.; Blanazs, A.; Battaglia, G.; Armes, S. P. *Macromolecules* **2012**, *45*, 5081.  
(39) Blanazs, A.; Madsen, J.; Battaglia, G.; Ryan, A. J.; Armes, S. P. *J. Am. Chem. Soc.* **2011**, *133*, 16581.  
(40) Battaglia, G.; Ryan, A. J. *J. Am. Chem. Soc.* **2005**, *127*, 8757.  
(41) Sugihara, S.; Blanazs, A.; Armes, S. P.; Ryan, A. J.; Lewis, A. L. *J. Am. Chem. Soc.* **2011**, *133*, 15707.  
(42) Li, Y.; Armes, S. P. *Angew. Chem., Int. Ed.* **2010**, *49*, 4042.  
(43) Mai, Y.; Eisenberg, A. *Chem. Soc. Rev.* **2012**, *41*, 5969.  
(44) Verber, R.; Blanazs, A.; Armes, S. P. *Soft Matter* **2012**, *8*, 9915.  
(45) Ladmiral, V.; Semsarilar, M.; Canton, I.; Armes, S. P. *J. Am. Chem. Soc.* **2013**, *135*, 13574.  
(46) Jones, E. R.; Semsarilar, M.; Blanazs, A.; Armes, S. P. *Macromolecules* **2012**, *45*, 5091.  
(47) Fielding, L. A.; Derry, M. J.; Ladmiral, V.; Rosselgong, J.; Rodrigues, A. M.; Ratcliffe, L. P. D.; Sugihara, S.; Armes, S. P. *Chem. Sci.* **2013**, *4*, 2081–2087.  
(48) Ratcliffe, L. P. D.; Ryan, A. J.; Armes, S. P. *Macromolecules* **2013**, *46*, 769.  
(49) Rawi, Z.; Mykytiuk, J.; Armes, S. P. *Colloids Surf.* **1992**, *68*, 215.  
(50) Thompson, K. L.; Armes, S. P.; Howse, J. R.; Ebbens, S.; Ahmad, I.; Zaidi, J. H.; York, D. W.; Burdis, J. A. *Macromolecules* **2010**, *43*, 10466.  
(51) Binks, B. P.; Whitby, C. P. *Langmuir* **2004**, *20*, 1130.  
(52) He, Y.; Wu, F.; Sun, X.; Li, R.; Guo, Y.; Li, C.; Zhang, L.; Xing, F.; Wang, W.; Gao, J. *ACS Appl. Mater. Interfaces* **2013**, *5*, 4843.  
(53) Walsh, A.; Thompson, K. L.; Armes, S. P.; York, D. W. *Langmuir* **2010**, *26*, 18039.  
(54) Williams, M.; Armes, S. P.; York, D. W. *Langmuir* **2011**, *28*, 1142.  
(55) Morse, A. J.; Dupin, D.; Thompson, K. L.; Armes, S. P.; Ouzineb, K.; Mills, P.; Swart, R. *Langmuir* **2012**, *28*, 11733.  
(56) Thompson, K. L.; Chambon, P.; Verber, R.; Armes, S. P. *J. Am. Chem. Soc.* **2012**, *134*, 12450.  
(57) Morse, A. J.; Armes, S. P.; Thompson, K. L.; Dupin, D.; Fielding, L. A.; Mills, P.; Swart, R. *Langmuir* **2013**, *29*, 5466.  
(58) Thompson, K. L.; Armes, S. P.; York, D. W.; Burdis, J. A. *Macromolecules* **2010**, *43*, 2169.  
(59) Binks, B. P. *Curr. Opin. Colloid Interface Sci.* **2002**, *7*, 21.  
(60) Two reviewers of this manuscript have pointed out that this is not the first time that model polymer-based Pickering emulsifiers have been prepared using PISA formulations. We are aware of three recent papers by An and co-workers on this topic: Chen, Q.; Cao, X.; Liu, H.; Zhou, W.; Qin, L.; An, Z. *Polym. Chem.* **2013**, *4*, 4092. Chen, Q.; Deng, X.; An, Z. *Macromol. Rapid Commun.* **2014**, *35*, 1148. Chen, Q.; Xu, Y.; Cao, X.; Qin, L.; An, Z. *Polym. Chem.* **2014**, *5*, 175.  
(61) Ahmad, S. A.; Wong, L. S.; Hobbs, J.; Leggett, G.; Micklefield, J. *J. Am. Chem. Soc.* **2009**, *131*, 1513.  
(62) DiFlavio, J.-L.; Pelton, R.; Leduc, M.; Champ, S.; Essig, M.; Frechen, T. *Cellulose* **2007**, *14*, 257.  
(63) Issa, R. M.; Khedr, A. M.; Rizk, H. *J. Chin. Chem. Soc.* **2008**, *55*, 875.  
(64) Yan, J.; Springsteen, G.; Deeter, S.; Binghe, W. *Tetrahedron* **2004**, *49*, 11205.